

Description of theoretical folds using differential geometry

Ian Mynatt^a, Raymond C. Fletcher^b, David D. Pollard^{a,*}

^aDepartment of Geological and Environmental Sciences, Stanford University, Stanford, CA, 94305

^bDepartment of Geosciences, Pennsylvania State University, University Park, PA 16803, USA

*dpollard@pangea.stanford.edu

Abstract

Through theoretical models of folded viscous layers, the effects of various loading conditions on fold geometry can be examined. We create models under both pure and simple shear loading conditions and quantify the resulting fold surface shapes using differential geometry. After calculating the absolute maximum and geologic curvature distributions across many modeled surfaces, it is shown that no difference in fold geometry based on loading conditions may be determined from the absolute maximum curvature distributions. However, distinct differences in the ratio of cylindrical to non-cylindrical points are evident between the simple and pure shear loading conditions and can be determined from the calculated geologic curvature of the surfaces. This application supplements and is based on the material found in Mynatt et al.(2007).

Low limb-dip surfaces created with folding theory

As a stiff layer embedded in a softer medium is deformed, for example, by bulk homogeneous shortening in-plane flow, and where the scale of this flow is much greater than the layer thickness, an array of three-dimensional folds will be created (Fig. 1). This complex three-dimensional surface results from initial perturbations in the layer's shape that are selectively amplified in the folding process based on the loading conditions. Using the approximate solution for folding at low limb-dip (Biot, 1961; Fletcher, 1977), we may follow the evolution of the upper surface of such a folded layer for the case of a single stiff viscous layer with viscosity η_l , embedded in a softer viscous medium with viscosity η_m .

It is well understood (e.g., Benjamin and Mullin, 1988; Fletcher, 1991) that in low limb-dip ($<15^\circ$) folding, appropriate periodic, cylindrical components in the surface shape are linearly independent, and the three-dimensional form of the surface is composed of the sum of

these component forms. The amplitudes, slopes, and orientations of these components are followed numerically using evolution equations such as those in Fletcher (1991), but modified for the different, cylindrical geometry of the components. We may then ask whether the characteristics of the differential geometry (e.g. distributions of curvatures) of such a surface is diagnostic of the type of basic-state flow, the viscosity ratio between the layer and the medium, $R = \eta_m / \eta_l$, or the stage in the evolution of the surface. Due to our selection of initial wavelengths the surface geometry will be independent of R except in terms of scale. Therefore we do not examine that variable here and assign all models a viscosity ratio of 0.05. Instead, we consider: a) two basic state flows; (i) simple shear; and (ii) pure shear with no extension normal to the plane of the layer; and b) the evolution of the surface over time given these loading conditions.

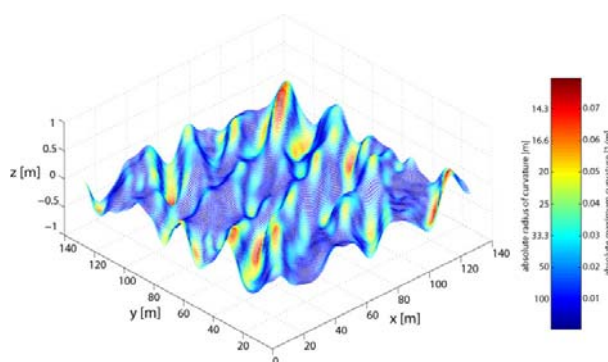


Figure 1. Three dimensional plot of the top of a theoretical folded viscous layer deformed by simple shearing with absolute maximum curvature mapped onto the surface. Note that only the magnitude and not the sign of the curvature is considered, so both synforms and antiforms have high values.

The basic state flows are induced by the application of uniform deformation rates, which are defined as the velocity gradients (Johnson and Fletcher, 1994). Simple shear is induced by:

$$D_{xx} = \frac{\partial v_x}{\partial x} = 0 ; D_{yy} = \frac{\partial v_y}{\partial y} = 0 ; D_{xy} = \frac{\partial v_x}{\partial y} = 1$$

In-plane pure shear is induced by:

$$D_{xx} = \frac{\partial v_x}{\partial x} = 1 ; D_{yy} = \frac{\partial v_y}{\partial y} = -1 ; D_{xy} = \frac{\partial v_x}{\partial y} = 0$$

In both cases:

$$D_{zz} = -(D_{xx} + D_{yy}) = 0$$

For each set of loading conditions and initial random perturbations, the surface is deformed starting at time zero (undeformed aside from the initial perturbations) in time steps Δt which sum to the total time of deformation, t_{fin} . In order to compare models starting from the same pseudo-random surface but subjected to different loading conditions, the amount of strain induced was used as the metric. For simple shear, the magnitude of maximum shortening (or the short axis of the unit strain ellipsoid e_3) is given by:

$$e_3 = \sqrt{1 + \frac{\gamma^2}{2} - \frac{\gamma}{2}\sqrt{4 + \gamma^2}}$$

Where $\gamma = 2D_{xy}t$ is the shear angle and t is time since application of the deformation rate D_{xy} . For pure shear:

$$e_3 = \exp(D_{xx}t)$$

For small values of t Eq. (4) and Eq. (5) are approximately equal. This allows for direct comparison of pure shear and simple shear models at the same time steps Δt , as long as the total time t_{fin} is relatively small, due to the fact that the amount of maximum shortening is approximately equivalent for the pure shear and simple shear cases at each time step.

Local slopes exceed $\sim 15^\circ$ at $t = 0.18$ (in arbitrary time units) so this is defined as t_{fin} . The total deformation time was divided into nine time steps, Δt , each 0.02. At t_{fin} the difference between the maximum shortening magnitudes is the greatest for the two loading conditions: e_3 for simple shear Eq. (4) is 0.8316 and 0.8353 for pure shear Eq. (5), suggesting the comparison of these loading conditions at each time step is appropriate.

Geometric description using differential geometry

Figure 2 shows the evolution of a given initial surface under both pure and simple shear. Figure 2a shows the undeformed state ($t = 0$) with a surface plot

(1) displaying the pseudo-random distribution of initial perturbations. The strain ellipse drawn on the surface is in its initial undeformed circular shape. The second plot in figure 2a shows the geologic curvature (2) value at each point on the surface, with the colors representing shapes as shown in figure 3. The third plot shows absolute maximum curvature which only (3) quantifies how “bent” the surface is at a given point without taking into account whether the curvature is convex or concave. Figure 1 shows a three dimensional fold with the absolute maximum curvature calculated across its surface. Note that synforms and antiforms both show high values, while limbs show low values. In figure 2a, both the geologic curvature and absolute maximum curvature appear to have more or less random distributions.

Figures 2d and 2e show the surface at $t = t_{fin} = 0.18$, under simple shear and pure shear (4) respectively. At this stage the surface plots show distinct corrugations across both surfaces, with the fold hinges sub-parallel to the long axes of the strain ellipses. These corrugations are the result of (5) amplification of cylindrical components oriented appropriately to the strain field (i.e. parallel to the long axis of the strain ellipse). The fold hinges can be seen in the geologic curvature and absolute maximum curvature plots as large continuous areas of mostly cylindrical points and sinuous linear features of high curvature value.

An important question to ask is whether the curvature distributions for the two loading conditions are different or, worded another way, can the loading conditions be inferred knowing something about the geometry of the deformed surface. The initial surface geometry influences the final geometry to a significant extent, so the effect of this variable needs to be minimized to answer the posed questions. Here we accomplish this by starting with 50 pseudo-random surfaces, subjecting them to both pure and simple shear and gathering the statistical distributions.

Starting at $t = 0$ and after each time step Δt the arithmetic mean of the mean, median, maximum and variance of the absolute maximum curvature was calculated for all 50 initial surfaces for both loading conditions. Also, the relative number of cylindrical (antiformal, synformal and planar) to non-cylindrical (basinal, domal and saddle) points for each model is calculated by dividing the total number of cylindrical points by the total number of non-cylindrical points. The curvature threshold was set so that the mean for the initial surfaces has a value of one for this relationship (i.e. the surface has an equal number of cylindrical and non-cylindrical points).

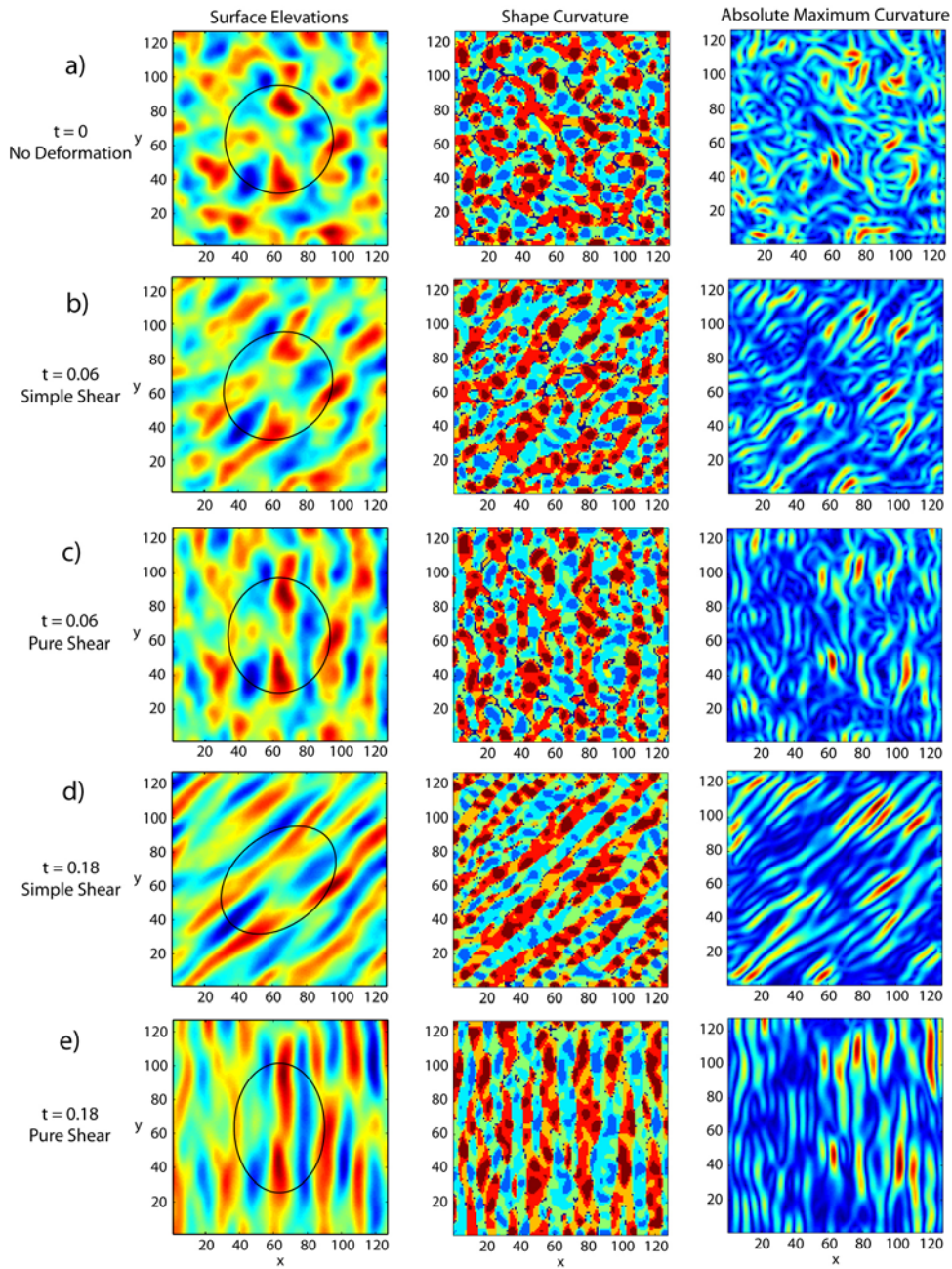


Figure 2. Evolution of a viscous layer subjected to a uniform deformation rate. The first column shows the elevation of the surfaces with red high values and blue low. Column two shows geologic curvature calculations color coded as in figure 3. Column three shows absolute maximum curvature calculations with red high values and blue low. a) The initial surface with pseudo-random perturbations. b) Simple shearing of the surface at $t = 0.06$. c) Pure shearing of the surface at $t = 0.06$. d) Simple shearing of the surface at $t = t_{fin} = 0.18$. e) Pure shearing of the surface at $t = t_{fin} = 0.18$.





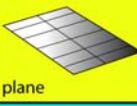



	$k_G < 0$	$k_G = 0$	$k_G > 0$
$k_M < 0$	 synformal saddle	 synform	 basin
$k_M = 0$	 perfect saddle	 plane	
$k_M > 0$	 antiformal saddle	 antiform	 dome

Figure 3. Geologic curvature classification. The geologic curvature of a point on a surface can be determined from the Gaussian (k_G) and mean (k_M) curvatures at the point. The color code seen here is used in figure 2. Modified from Roberts (2001) and Bergbauer (2002).

Discussion

While the absolute maximum curvature distribution may be statistically different for two loading conditions applied to the same initial surface, we have shown that after removing the effect of the initial surface geometry there is virtually no difference between the pure and simple shear cases. However, the ratio of cylindrical to non-cylindrical points does show significant differences between the two loading conditions (Fig. 4). While both loading conditions show an increase in the number of non-cylindrical points as the surface evolves, this increase is greater for the simple shear case. If one knew the model parameters (e.g. viscosity, total time, strain magnitude etc.) but not the loading style, one could calculate the ratio of cylindrical to non-cylindrical points on the surface and determine whether the structure had formed in simple or pure shear.

Acknowledgements

Raymond C. Fletcher acknowledges support from American Chemical Society PRF grant number 40877-AC8.

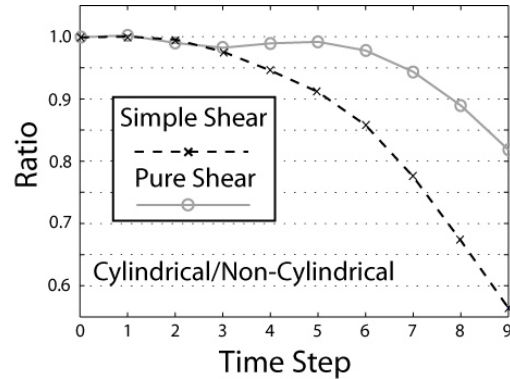


Figure 4. The averaged ratio of cylindrical to non-cylindrical points for simple and pure shear loading of 50 initial surfaces. Note this ratio starts at one in the initial state ($t = 0$).

References

- Benjamin, T. B., and T. Mullin, 1988, Buckling instabilities in layers of viscous-liquid subjected to shearing: *Journal of Fluid Mechanics*, v. 195, p. 523-540.
- Bergbauer, S., 2002, The use of curvature for the analysis of folding and fracturing with application to the Emigrant Gap Anticline, Wyoming: Ph. D. thesis, Stanford University, 216 p.
- Biot, M. A., 1961, Theory of folding of stratified viscoelastic media and its implication in tectonics and orogenesis: *Geological Society of America Bulletin*, v. 72, p. 1595-1620.
- Fletcher, R. C., 1977, Folding of a single viscous layer: exact infinitesimal amplitude solution: *Tectonophysics*, v. 39, p. 593-606.
- Fletcher, R. C., 1991, Three-dimensional folding of an embedded viscous layer in pure shear: *Journal of Structural Geology*, v. 13, p. 87-96.
- Johnson, A. M., and R. C. Fletcher, 1994, *Folding of Viscous Layers*: New York, Columbia University, 461 p.
- Mynatt, I., S. Bergbauer, and D. D. Pollard, 2007, Using differential geometry to describe 3-D folds: *Journal of Structural Geology*, v. in press.
- Roberts, A., 2001, Curvature attributes and their application to 3D interpreted horizons: *First Break*, v. 19, p. 85-100.